



Published in final edited form as:

Cell. 2008 January 11; 132(1): 113–124.

PTRF-cavin, a conserved cytoplasmic protein required for caveola formation and function

Michelle M. Hill^{1,2}, Michele Bastiani^{1,2,3}, Robert Luetterforst^{1,2,3}, Matthew Kirkham^{1,2,3,4}, Annika Kirkham^{1,2,3,5}, Susan J. Nixon^{1,2}, Piers Walser^{1,2}, Daniel Abankwa¹, Viola M. J. Oorschot^{1,2,6}, Sally Martin^{1,2}, John F. Hancock¹, and Robert G. Parton^{1,2,*}

¹ Institute for Molecular Bioscience, University of Queensland, Brisbane, Queensland 4072, Australia.

² Centre for Microscopy and Microanalysis, University of Queensland, Brisbane, Queensland 4072, Australia.

Summary

Caveolae are abundant cell surface organelles involved in lipid regulation and endocytosis. We used comparative proteomics to identify PTRF (also called Cav-p60, Cavin) as a putative caveolar coat protein. PTRF-cavin selectively associates with mature caveolae at the plasma membrane but not Golgi-localized caveolin. In prostate cancer PC3 cells, and during development of zebrafish notochord, lack of PTRF-cavin expression correlates with lack of caveolae, and caveolin resides on flat plasma membrane. Expression of PTRF-cavin in PC3 cells is sufficient to cause formation of caveolae. Knockdown of PTRF-cavin reduces caveolae density, both in mammalian cells and in the zebrafish. Caveolin remains on the plasma membrane in PTRF-cavin knockdown cells but exhibits increased lateral mobility and accelerated lysosomal degradation. We conclude that PTRF-cavin is required for caveolae formation and sequestration of mobile caveolin into immobile caveolae.

Keywords

caveolin; PTRF; cavin; zebrafish; prostate cancer

Introduction

Caveolae are a characteristic and abundant morphological feature of many mammalian cells. Caveolae have been implicated in numerous functions including cell signaling, lipid regulation, and endocytosis. The only known structural proteins of caveolae are members of the caveolin family, caveolin-1 (Cav1), caveolin-2 (Cav2) and caveolin-3 (Cav3). Cav1 is expressed in non-striated muscle cells and drives caveolae formation. Caveolae are absent from non-muscle tissues of Cav1^{-/-} animals (Drab et al., 2001) and ectopic expression of Cav1 in cells lacking caveolae leads to de novo caveolae formation (Fra et al., 1995). Cav3 is expressed in skeletal and cardiac muscle (Pol et al., 2005; Way and Parton, 1995), and is required for caveolae formation in these cells (Galbiati et al., 2001; Hagiwara et al., 2000). In contrast, Cav2 is not

³These authors contributed equally to this work

⁴Current address: Department of Cell and Molecular Biology, Karolinska Institute, 17177 Stockholm, Sweden.

⁵Current address: Biovitrum AB, SE-112 76 Stockholm, Sweden.

⁶Current address: Cell Microscopy Center, Department of Cell Biology, University Medical Center Utrecht, The Netherlands.

*Contact: r.parton@imb.uq.edu.au

Publisher's Disclaimer: This is a PDF file of an unedited manuscript that has been accepted for publication. As a service to our customers we are providing this early version of the manuscript. The manuscript will undergo copyediting, typesetting, and review of the resulting proof before it is published in its final citable form. Please note that during the production process errors may be discovered which could affect the content, and all legal disclaimers that apply to the journal pertain.

Additional Experimental Procedures are available as Supplemental text.

required for caveolae formation (Razani et al., 2002) and its transport to the plasma membrane is dependent on Cav1 expression (Parolini et al., 1999). Cav1 binds cholesterol (Murata et al., 1995) and forms higher order oligomers (Monier et al., 1996). These properties are believed to be important for generation of the characteristic structure of caveolae, each of which contains approximately 144 caveolin molecules (Pelkmans and Zerial, 2005). Caveolae may be generated in the Golgi complex, as a unit which fuses directly with the plasma membrane (Tagawa et al., 2005). While the role of caveolin in caveolae formation is therefore well-established (Parton et al., 2006), it is not known whether other proteins are required for caveolae formation or if they can regulate the balance between caveolae formation and disassembly.

Caveolae play an important role in the regulation of many cellular functions. For example, down-regulation of Cav1 has been correlated with cell transformation and tumour invasion (Williams and Lisanti, 2005). Precisely how caveolae/caveolins regulates cellular processes remains unclear. In contrast to the dynamic transient nature of many signal transduction complexes, caveolae are generally extremely stable structures (Tagawa et al., 2005; Thomsen et al., 2002). The caveolar unit stays intact despite cycles of endocytosis, fusion with the caveosome or endosomes, and recycling back to the plasma membrane (Pelkmans and Zerial, 2005). However, caveolin becomes mobile upon cholesterol depletion and a large scale screen identified kinases which when downregulated cause significant changes in caveolin distribution (Pelkmans et al., 2005). This suggests that the formation of the caveolar unit may be regulated.

To gain further insights into caveolar function we utilized comparative proteomics of Cav1^{-/-} and wild type (WT) mouse embryonic fibroblasts and found Polymerase I and Transcript Release Factor, PTRF, to be targeted to detergent-resistant membranes (DRM) in a Cav1-dependent manner. PTRF, also called Cav-p60 or Cavin, was previously localized to caveolae by the group of Trantum-Jensen using antibodies derived from rat adipocyte membranes (Vinten et al., 2005; Vinten et al., 2001; Voldstedlund et al., 2003; Voldstedlund et al., 2001). More recently, PTRF was identified as a component of immunopurified caveolae from human adipocytes (Aboulaich et al., 2004). PTRF is a soluble protein with putative leucine zipper, nuclear localization sequences and PEST domains (Aboulaich et al., 2004; Gustincich et al., 1999). We now show that PTRF-cavin is required for formation of caveolae in cultured cells and zebrafish embryo.

Results

Analysis of DRM from WT and Cav1^{-/-} MEFs reveal minor differences in presence/absence of caveolin

In order to identify putative caveolae proteins, we employed a comparative proteomic screen using detergent-resistant membranes (DRM) prepared from WT and Cav1^{-/-} murine embryonic fibroblasts (MEFs). While DRM do not equate to caveolae or lipid raft domains (Lichtenberg et al., 2005), this strategy represents a non-biased approach to identify proteins recruited to this fraction, directly or indirectly, by caveolin. Since Cav1^{-/-} cells are devoid of morphological caveolae, proteins that are absent in Cav1^{-/-} DRM compared to WT DRM are expected to be components of caveolae. As shown in Figure 1, the protein profile for WT and Cav1^{-/-} DRM are extremely similar, both on SDS-PAGE (Figure 1A) and on 2DE (Figure 1B), consistent with the fact that caveolae proteins represent only a minor proportion of the total DRM proteins.

To identify proteins specific to WT DRM, gel slices were excised from entire lanes of Coomassie-stained SDS-PAGE, digested with trypsin and analyzed by MS/MS. After two independent TOF-TOF analyses, 53 common proteins were identified in WT and Cav1^{-/-} DRM, while 8 proteins were found to be preferentially enriched in WT DRM and 6 proteins

enriched in Cav1^{-/-} DRM. Polymerase I and Transcript Release Factor (PTRF) was identified as a protein preferentially enriched in WT DRM (Figure 1C). In addition, a related protein, Serum-deprivation response protein (SDPR) was also found enriched in WT DRM (Figure 1C).

Consistent with the proteomic data, western blotting showed that a PTRF immunoreactive band of 60 kDa was significantly reduced in Cav1^{-/-} DRM (Figure 1D). This difference was consistently observed in numerous DRM preparations, while the abundance of many other signaling proteins were found to be similar between WT and Cav1^{-/-} DRM, including eNOS, Src, PKB and Fyn (Figure 1D). Indeed, the only signalling protein we found to target to DRM in a Cav1-dependent manner was protein kinase C α (PKC α , Figure 1D). To examine whether the reduction of PTRF in Cav1^{-/-} DRM is a result of an overall reduction in PTRF protein, we performed immunoblotting for PTRF in MEF whole cell lysates, as well as lysates of adult mouse tissues (Figure 1E). The expression of PTRF was similar in WT and Cav1^{-/-} MEF whole cell lysates (Figure 1E). In adult mouse tissues, PTRF showed an expression pattern that strictly correlated with caveolin, with highest expression in lung, fat and adrenal gland, and intermediate expression in heart and skeletal muscle (Figure 1E). A second PTRF-immunoreactive band at 25 kDa was detected in mouse tissues but not in MEFs (Figure 1E). The intensity of this band paralleled that of full-length PTRF in most tissues, suggesting that it may be a degradation product, possibly corresponding to the reported cleaved PTRF (Aboulaich et al., 2004). Intriguingly, PTRF expression is dramatically reduced in Cav1^{-/-} adult mouse tissues (Figure 1E), strongly suggesting that these two proteins are functionally linked.

PTRF associates with caveolae

PTRF was recently identified as a component of immunopurified caveolae from human adipocytes (Aboulaich et al., 2004), and as cav-p60, a protein previously localized to rat adipocyte caveolae (Vinten et al., 2005). To confirm the subcellular localization of PTRF in fibroblasts, we performed immunofluorescence (IF) confocal microscopy in WT MEF and NIH 3T3 cells. In addition to a cytosolic pool, PTRF showed punctate cell surface staining which colocalized with Cav1-enriched regions of the plasma membrane (Figure 2A and 2B). Detailed analysis of the confocal images revealed that all plasma membrane Cav1 puncta were co-labelled with PTRF, whereas a small number of Cav1-free PTRF puncta could also be detected. To confirm that PTRF is localizing to caveolae, we performed immunoelectron microscopy (immuno-EM) on plasma membrane lawns (Prior et al., 2003) generated from baby hamster kidney (BHK) cells co-transfected with Cav1-mGFP and PTRF-RFP. Cav1 and PTRF were detected by GFP and RFP antibodies coupled to 6 nm and 2 nm gold respectively. As shown in Figure 2C, Cav1 and PTRF both labelled caveolae although low levels of expressed PTRF were also detected on flat membrane.

By IF, Cav1^{-/-} MEF showed a diffuse distribution of either endogenous or ectopically expressed PTRF (Figure 2D,E), consistent with limited plasma membrane association or binding to flat membrane. To determine whether the alteration of PTRF subcellular localization in Cav1^{-/-} MEF was a direct result of loss of Cav1, Cav1 was re-expressed in Cav1^{-/-} MEF. Immunoblotting showed that expression of Cav1 caused recruitment of PTRF to the DRM fraction (Figure 3A) and IF analysis showed recruitment of PTRF to caveolin-enriched puncta at the plasma membrane (Figure 3B). These results show that Cav1 is necessary and sufficient to recruit PTRF to the plasma membrane.

In addition to the cell surface, caveolins are also present in the Golgi complex in many cells, corresponding to a pool of newly-synthesized protein (Nichols, 2002; Pol et al., 2005). As Cav1 recruits PTRF to the plasma membrane we investigated whether PTRF is also recruited to the Golgi complex. Endogenous PTRF colocalized with Cav1 at the plasma membrane but

not at the Golgi complex in WT MEF (Figure 2A) and NIH 3T3 fibroblasts (Figure 2B). Expression of Cav1 or Cav3 in Cav1^{-/-} MEFs is sufficient to generate caveolae (Kirkham et al., 2005). Expression of Cav1 (Figure 3B), or Cav3 (Figure 3C) in Cav1^{-/-} MEFs also caused the recruitment of PTRF to the plasma membrane, but not the Golgi complex (arrowheads in Figure 3C). To further characterize this apparent selectivity for caveolin at the plasma membrane, we examined a series of caveolin mutants with different subcellular localizations. Golgi-associated mutants of Cav3, such as Cav3P104L, were unable to recruit PTRF (Figure 3D). Another mutant, Cav3C71W, which localizes both to the cell surface (to generate caveolae; unpublished results), and the Golgi complex shows recruitment of PTRF to the cell surface but not to the Golgi complex (Figure 3E; arrowhead).

To further clarify the requirement of caveolae formation in PTRF recruitment, we assessed the ability of caveolins from different species – ranging from mammals to invertebrates - to recruit PTRF. In agreement with the results from caveolin mutants, there was a strict correlation between caveolae formation and PTRF recruitment (Figure 3F-H). Caveolin from *C. elegans*, which is also surface localized, but is unable to generate caveolae, did not recruit PTRF to the plasma membrane (Figure. 3F). In contrast, zebrafish caveolin generated caveolae and recruited PTRF to the plasma membrane (Figure 3H). Remarkably, an invertebrate caveolin from the honey bee *A. mellifera*, which generated caveolae caused PTRF recruitment (Figure. 3G). Hybrid proteins between mammalian and CeCav also showed the same correlation between caveolae formation and PTRF recruitment (Figure S2), further strengthening the conclusion that only plasma membrane caveolar caveolin recruits PTRF.

PTRF and caveolin are in close proximity at the plasma membrane

The above results prompted us to examine the possible interaction between PTRF and caveolin. We employed the in situ techniques of sensitized acceptor emission and fluorescence lifetime imaging (FLIM) and fluorescence resonance energy transfer (FRET) to examine whether PTRF and caveolin are in close proximity. For FRET studies, monomeric fluorescent proteins were used to tag PTRF and Cav1, and then co-transfected into BHK cells. FRET was detected in vesicular structures which lined the plasma membrane and were also distributed in the cell periphery (Figure 4A, see also Figure S3). All structures where mCFP-PTRF and Cav1-mCitrine colocalized displayed FRET with an efficiency of 10-20%. For FLIM studies, mGFP-PTRF was transfected into BHK cells or co-transfected with mRFP-Cav3 and its fluorescence lifetime measured. The fluorescence lifetime of mGFP-PTRF was significantly reduced ($p < 0.0001$) when mRFP-Cav3 was co-expressed (Figure 4B). We further estimate that approximately 20% of PTRF molecules are sufficiently proximate to an mRFP-Cav3 acceptor molecule to undergo FRET (Figure 4B). Taken together, these results show that PTRF and caveolin are closely associated at the plasma membrane.

To gain additional insights into the mechanism of PTRF recruitment to caveolae, we estimated the stoichiometry of PTRF recruitment to DRM by caveolin. mGFP-PTRF and Cav3-mGFP were co-transfected in Cav1^{-/-} MEF at a ratio of 3:1, so that all cells expressing mGFP-PTRF should express Cav3-mGFP. DRMs were prepared and examined by immunoblotting with anti-GFP antibody. As expected, co-transfection of Cav3-mGFP with mGFP-PTRF caused a recruitment of mGFP-PTRF to the DRM (Figure S4). In control dishes where GFP was used in place of Cav3-mGFP, only a trace amount of mGFP-PTRF was detected in the DRM (Figure S4). Quantitative immunoblotting estimated the ratio of Cav3-mGFP to mGFP-PTRF in the DRM to be 5.5 ± 1.9 (range between 2.1 to 8.6, $n=3$). The high variation of estimates obtained with this method may be due to dissociation of PTRF during preparation of DRM, and prompted us to perform an independent, fluorescence-based assay to refine the estimates of the PTRF:caveolin stoichiometry. NIH 3T3 cells transfected with either Cav3-mGFP or PTRF-mGFP, were imaged by confocal microscopy using the same capture conditions in each case.

Mean grey level values were measured for particles which fitted within a $0.177 \mu\text{m}^2$ circle, with the assumptions that each puncta correspond to one caveola, and that contribution of endogenous caveolin/PTRF in caveolae is negligible upon high overexpression. The mean grey level value for Cav3 and PTRF was 22.28 ± 0.46 ($n=127$) and 23.45 ± 0.62 ($n=100$), suggesting that caveolin and PTRF are present in an approximate 1:1 ratio within caveolae.

Co-immunoprecipitation of PTRF with Cav1, with and without *in vivo* crosslinking, using either PTRF, caveolin, GFP or Flag antibodies under different solubilization conditions provided equivocal results (data not shown). This raises the possibility that PTRF associates with the specific lipid environment generated by caveolin. Cav1 binds cholesterol (Murata et al., 1995) and depletion of cellular cholesterol results in a loss of morphological caveolae (Hailstones et al., 1998). To determine if PTRF-caveolin interaction requires cholesterol, we used methyl- β -cyclodextrin to extract cholesterol, and then examined the interaction by FLIM. Cholesterol depletion to $\sim 50\%$ attenuates PTRF-caveolin interaction as measured by an increase in the fluorescence life-time of mGFP-PTRF (Figure 4C), correlating with the reported loss of morphological caveolae under these conditions (Hailstones et al., 1998). PTRF shares sequence homology with SDPR and SRBC, both of which have been shown to bind phosphatidylserine (PS) (Burgener et al., 1990; Gustincich et al., 1999; Izumi et al., 1997) and caveolin peptides have been reported to generate PS-rich domains *in vitro* (Wanaski et al., 2003). We therefore examined if PTRF could bind PS *in vitro*. Recombinant PTRF bound pure PS in a solid phase assay, with the interaction completely lost when phosphatidylcholine (PC) was included at a 50 fold excess (Figure 4D). This interaction was further confirmed using a liposome centrifugation assay (Figure 4E). Taken together the results suggest that PTRF is a PS-binding protein which is recruited to caveolae in a cholesterol-dependent manner, and is an abundant component of caveolae.

PTRF is required for caveolae formation in PC3 cells

In view of the strict association of PTRF with caveolae, we tested the hypothesis that PTRF aids caveolae formation. Screening a panel of cell lines revealed that protein levels of PTRF and Cav1 closely parallel each other in most cell lines (data not shown), with the exception of the prostate cancer cell line PC3, which expressed abundant Cav1 but no detectable PTRF (Figure 4F). By IF, caveolin showed a diffuse staining in PC3 cells (Figure 4G, cell on right), similar to *C. elegans* caveolin (Figure 3F) which targets to the plasma membrane but does not form caveolae. In agreement with this, electron microscopic analysis of ruthenium red surface-labeled cells showed extremely low levels of morphologically-recognisable caveolae (Figure 4H; occupying $<0.2\%$ of the plasma membrane surface as estimated by sterology). Transfection of PTRF caused a dramatic change in Cav1 distribution by IF, with large puncta now visible in the transfected cells (Figure 4G, cell on left). The transfected cells were processed for electron microscopy (Figure 4H) and caveolae density in the transfected cell population was quantitated in a blind fashion in comparison to control cells. Although the transfection efficiency was less than 50%, the caveolae density dramatically increased upon PTRF transfection with a 6.5 fold increase as measured over the entire population (0.26 ± 0.13 caveolae per field to 1.70 ± 0.94). Caveolae were evident as single structures on the plasma membrane and in the characteristic surface-connected 'caves' or rosette structures described in many cell types (Figure. 4H). We conclude that PTRF is limiting for caveolae formation in this prostate cancer cell line.

Downregulation of PTRF causes loss of surface caveolae

To further test the role of PTRF in caveolae formation, NIH 3T3 fibroblast cell lines with reduced PTRF levels were generated by stable expression of shRNA (shPTRF) and compared to control lines generated in parallel with either a scrambled shRNA vector, or shRNA directed against Cav3 (shCON, note that Cav3 is not expressed in NIH 3T3 fibroblasts). A reduction

of PTRF expression by 80-95% caused a 10-50% reduction of Cav1 protein levels in different cell lines (an example is shown in Figure 5A), however, the majority of Cav1 still localized to the DRM fraction (Figure 5A). By IF, endogenous Cav1 showed a diffuse surface distribution in shPTRF cells (Figure 5B), in contrast to the characteristic linear and/or punctate distribution in parental NIH 3T3 fibroblasts (Figure 2B) or shCON cells (Figure 5B). Importantly, we were able to restore the characteristic Cav1 staining pattern in shPTRF cells by re-expressing GFP-PTRF to high levels to partially overcome the shRNA inhibition (Figure 5C).

To examine the effect of PTRF knockdown on caveolae, we used ruthenium red to label the cell surface of shCON and shPTRF cells. Control cells showed abundant 60-80nm invaginations of the cell surface, characteristic of caveolae (Figure 5D). In contrast, caveolae were rare in shPTRF cells (Figure 5E). This was quantitated in a blind fashion using two independent methods, and compared to the level of caveolae observed in Cav1 knockdown cells generated using shRNA in NIH 3T3 cells (Figure S5). The percentage of the cell surface occupied by caveolae decreased from $10.9 \pm 1.11\%$ ($n=76$ fields) in shCON cells to $3.45 \pm 0.43\%$ ($n=65$ fields) in shPTRF cells and $2.60 \pm 0.64\%$ in shCav1 cells ($n=54$ fields), as measured by standard stereological methods on random sections. Similar results were obtained by independent quantitation of caveolae numbers per field in random areas of the cell surface. This corresponds to a decrease of caveolae density of 68% upon PTRF downregulation, as compared to 76% upon Cav1 knockdown using similar methods and quantitated in parallel. There was no evidence of abnormal caveolae formation in either case.

To investigate the distribution of Cav1 in shPTRF cells we performed quantitative immunocytochemistry (EM) on frozen sections. In control cells (shCON) the majority of Cav1 labeling ($81.7 \pm 4.6\%$ of surface labeling) was associated with 65nm vesicles close to, or clearly connected to the plasma membrane (Figure 6A,B). In contrast, in shPTRF cells the bulk of plasma membrane labeling was associated with non-caveolar plasma membrane ($79.1 \pm 5.3\%$; Figure 6C-E). The remaining 21% of surface gold associated with caveolae may reflect the incomplete knockdown of PTRF. Total labeling for Cav1 (gold particles per random field) was decreased approximately 25% in shPTRF cells, although it is important to note that we cannot assume similar labeling efficiency for Cav1 in caveolae and flat plasma membrane. To our surprise, in shPTRF cells, a significant, although low, fraction of Cav1 was observed in clathrin coated pits (see example inset Figure S7A). Although less than 1% of total Cav1 labeling, the significance of this association was indicated by the total absence of Cav1 labeling in clathrin coated pits of shCON cells labeled in parallel. Consistent with association of Cav1 with the endocytic pathway upon PTRF downregulation, Cav1 labeling was observed in endocytic structures, including multivesicular putative late endosomes in shPTRF cells but not in shCON cells (Figure S7A,B). Together with the observed decrease in Cav1 levels, this raised the possibility that PTRF knockdown could allow Cav1 to be internalized and degraded. Consistent with this, cycloheximide chase experiments showed significant degradation of Cav1 within 6-8h in shPTRF cells but not shCON cells (Figure 6F). This downregulation of Cav1 was completely inhibited by treatment with lysosomal inhibitors (results not shown). The low level of labeling of the Golgi complex, was similar in control and shPTRF cells (Figure S7C,D) consistent with the hypothesis that the principal role for PTRF is to stabilise caveolin at the plasma membrane rather than facilitate Golgi exit.

Caveolin in caveolae are reported to be relatively immobile, but can be mobilized upon cholesterol depletion (Thomsen et al., 2002). To examine if release of caveolin by PTRF knockdown has a similar effect, we performed FRAP (fluorescence recovery after photobleaching) analysis on yellow fluorescent protein (YFP)-tagged Cav1 transfected in shCON versus shPTRF cells (Figure 6G). Consistent with previous reports (Thomsen et al., 2002), Cav1-YFP mobility was extremely low in control cells, with an immobile fraction of 0.778 (Figure 6B). The immobile fraction of Cav1-YFP in shPTRF cells was significantly

decreased to 0.369 (Figure 6B), reminiscent of that seen in cholesterol-depleted cells (Thomsen et al., 2002). In contrast, the half life of fluorescence recovery was not significantly different in the two cell lines. The mobile fraction in each cell type (22% and 63% for shCON and shPTRF respectively) are not significantly different ($\tau^2=1.45$, $p=0.228$) to the percentage of non-caveolar Cav1 observed in the immuno-EM analysis (18% and 79% respectively).

Taken together these results suggest that PTRF is required to stabilize caveolin in caveolae at the plasma membrane. Loss of PTRF causes caveolin to diffuse freely in the plasma membrane and to become internalized (presumably as a passive bulk flow marker) into the endolysosomal system where degradation occurs. These data agree with a model in which sequestration of caveolin into caveolae, promoted by PTRF, causes stable confinement of caveolin, thus protecting it from degradation.

PTRF is required for caveolae formation and notochord structure in zebrafish

In order to determine whether PTRF was also required for caveolae formation *in vivo* we made use of the zebrafish, *Danio rerio*. We have recently demonstrated the high expression of Cav1 and caveolae in the notochord of the zebrafish embryo (Nixon et al., 2007). Formation of caveolae in the notochord occurs early in development and notochord caveolae are highly abundant and easily quantified. Since gene expression can be readily ablated using morpholino (MO) technology at this stage of development, this offers a powerful *in vivo* system to study caveolae formation. The cDNA for the putative zebrafish PTRF was cloned by PCR based on a predicted protein from Ensembl, transcript number GENSSCAN00000026855. The sequence has been submitted to Genbank (accession number EF633994). The putative zebrafish PTRF protein is 50% identical and 62% similar to human PTRF.

The zebrafish PTRF homolog was clearly detected within the notochord at 18h to 31h post fertilization by *in situ* hybridization (Figure 7), overlapping with the expression of Cav1 (Fang et al., 2006; Nixon et al., 2007). In addition, at later stages of development, expression of PTRF could be detected in blood vessels, branchial arches and otic vesicles (Figure 7C). PTRF expression was first detected in the notochord of 18h embryos (Figure 7F,G), with labelling absent in 16h embryos (Figure 7D,E). This was of high interest as Cav1 expression was detected as early as 12h (Figure. 7I) (Fang et al., 2006; Nixon et al., 2007). The differential expression of PTRF and Cav1 transcripts in early zebrafish embryos was confirmed by RT-PCR (Figure 7H), and we further confirmed the expression of Cav1 protein by immunohistochemistry in 16h embryos (Figure 7J). Notochord ultrastructure from 16h and 24h embryos was examined by electron microscopy (Figure S8). In agreement with our previous data, morphological caveolae were not detectable at 16h, but was highly abundant at 24h, again supporting a role for PTRF in caveolae formation.

To examine whether PTRF is required for caveolae formation in the zebrafish, we performed PTRF knockdown in zebrafish embryos. Injection of PTRF-MO produced a curved phenotype in 42% of the injected embryos (Figure 7K,L), identical to the curved phenotype observed in Cav1-MO zebrafish embryos (Nixon et al., 2007). Similar results were obtained using a splicing-blocking MO. Quantitation of caveolae density in the notochord of PTRF-MO and control-MO zebrafish showed a dramatic reduction in caveolae upon PTRF downregulation (Figure 7M,N). Caveolae density correlated with the severity of phenotype (mild $43.7 \pm 5.5\%$ of caveolae in the notochord of control MO-injected embryos; severe $23.6 \pm 3.6\%$ of control). The level of caveolae reduction is comparable to that reported for Caveolin-MO (Fang et al., 2006; Nixon et al., 2007). We examined the localization of Cav1 in PTRF-MO embryos by immuno-EM (Figure 7O-Q). In control-MO notochord, the plasma membranes between two adjacent cells are tightly opposed and contain numerous Cav1-decorated caveolae (Figure 7O). In contrast, gaps can be observed between neighbouring notochord cells in PTRF MO-injected embryos (Figure 7N), and Cav1 labelling is mainly associated with flat membrane (Figure 7

P,Q). These results show that PTRF is required for caveolae formation *in vivo* and that this role is conserved in evolution.

Discussion

In this study we have shown that PTRF, a protein initially identified as a transcript release factor is required for caveola formation in mammals and the zebrafish. We suggest that the name PTRF-cavin would be more appropriate for this protein. PTRF-cavin shows unique properties; it associates with mature caveolae at the plasma membrane but does not associate with non-caveolar caveolin (in the Golgi complex, or with mutant forms of caveolin). This interaction is conserved in evolution; mammalian PTRF-cavin even associates with caveolae generated by expression of invertebrate caveolins. PTRF-cavin, unlike caveolin, is a soluble cytosolic protein recruited to the membrane to generate caveolae. Together with the abundance of PTRF-cavin in caveolae, this suggests that PTRF-cavin operates as a coat protein for caveolae.

The current model of caveolae biogenesis suggests that caveolae form at the Golgi complex, in a process involving caveolin oligomerization and cholesterol binding, and traffic as a unit which fuses directly with the plasma membrane (Tagawa et al., 2005). Once at the plasma membrane, caveolae are relatively immobile but can be endocytosed, to be recycled or fuse with the endosome or the caveosome (Kirkham et al., 2005; Pelkmans et al., 2002; Thomsen et al., 2002). A unique feature of the caveolar domain as illustrated in these studies, was the maintenance of the stable caveolar unit despite multiple rounds of endocytic transport. This is quite different to the assembly and disassembly of coat components of classical coated structures such as clathrin-coated vesicles. In agreement with this model, we did not detect a change in PTRF-cavin/caveolin interaction upon stimulation of caveolae endocytosis (data not shown).

Individual caveolae were estimated to each contain 144 molecules of caveolin (Pelkmans and Zerial, 2005). PTRF-cavin is also clearly an abundant component of caveolae as shown here and suggested in previous studies based on immunogold labeling density (Voldstedlund et al., 2001). High ectopic expression of caveolin results in association of caveolin with non-caveolar domains where it shows higher lateral mobility (Pelkmans and Zerial, 2005). PTRF-cavin may be one component which becomes limiting under these conditions, since downregulation of PTRF-cavin causes a loss of caveolae but caveolin remains at the plasma membrane and associated with DRMs. The possibility that the caveolar unit can be disassembled, through dissociation of PTRF, to release caveolin and other sequestered components in the bulk membrane can now be examined.

How does PTRF recognize and stabilize caveolae? While we can show close association of caveolin and PTRF-cavin, our inability to consistently detect their stable association using immunoprecipitation techniques raises the possibility of an indirect role of caveolin and the potential involvement of membrane lipids. We have now shown binding of recombinant PTRF-cavin with PS *in vitro* (Figure 4D,E) and a requirement for cholesterol for PTRF-cavin/caveolin interaction (Figure 4C). As the caveolin scaffolding domain has been proposed to oligomerize *in vitro* to form lateral membrane domains containing PS and cholesterol (Wanaski et al., 2003), an intriguing possibility is that PTRF-cavin binds caveolin-generated PS-cholesterol domains, thus stabilizing the membrane curvature of caveolae. This is consistent with the fact that even an invertebrate caveolin, with limited sequence conservation, when expressed in mammalian cells can recruit PTRF-cavin. Our results suggest a model where caveolae biogenesis would primarily involve caveolin-driven domain formation, but with PTRF-cavin providing critical stability for the nascent caveolar structures. Whether the mechanisms involved show any similarities to the generation of curvature in other systems, such as those driven by BAR domain proteins (Dawson et al., 2006) will await further detailed investigation

of the cooperation between caveolin and PTRF-cavin, and a detailed understanding of the membrane lipid-protein interactions involved.

Conclusions

In this study, we have defined PTRF-cavin as an essential component of caveolae. We propose a new model of caveolae formation and function in which PTRF-cavin is recruited to membrane domains containing PS, cholesterol and oligomerized caveolins. Binding of PTRF-cavin to these domains stabilizes the membrane curvature to produce the classic flask shape of caveolae. Loss of PTRF-cavin releases caveolar components, including caveolins into the plasma membrane. The level of non-caveolar caveolins are tightly regulated via endolysosomal degradation. PTRF-cavin is therefore a potential caveolar coat protein that regulates caveola structure and function.

Experimental Procedures

Electron microscopy and quantitation

Labelling of the cell surface by ruthenium red fixation was performed as previously described (Parton et al., 2002). The % area of the cell surface occupied by caveolae was estimated by intersection counting as in previous studies (Parton, 1994) except that counting was performed on captured images (Jeol 1011 TEM equipped with Morada cooled CCD camera and Olympus Soft Imaging Solutions GmbH, Germany with AnalySIS software) at a magnification of 15-20,000x. Images were captured at random from different areas of the monolayer and overlaid with appropriate double lattice grids to measure intersections with the plasma membrane (25x grid) and with caveolae (1x grid) defined as 60-100nm uncoated invaginations of the ruthenium red-labeled plasma membrane. 2 independent fields from each of at least 2 independent experiments were quantitated for each condition and similar results were obtained in double blind experiments in which codes were broken after quantitation.

FRET-imaging

FRET was measured as sensitised acceptor emission using the three-cube method as previously described (Erickson, 2001). Images in donor (ex 405 nm, em 470-500 nm), acceptor (ex 514 nm, em 530-600 nm) and FRET (ex 405 nm, em 530-600 nm) channels were acquired on a Zeiss LSM 510 Meta using a 63x or 100x oil immersion objective, with numerical apertures of 1.4. Living cells were imaged in PBS/1mM CaCl₂.

FLIM

FLIM experiments were carried out using a lifetime fluorescence imaging attachment (Lambert Instruments, Leutingwolde, The Netherlands) on an inverted microscope (Olympus IX71). BHK cells transiently expressing mGFP-PTRF (donor), alone or with mRFP-Cav3 (acceptor) (using a 1:3 ratio of plasmid DNA) were excited using a sinusoidally modulated 3W 470nm LED at 80MHz under epi-illumination. Fluorescein was used as a lifetime reference standard. Cells were imaged with a 60x NA 1.45 oil objective using an appropriate GFP filter set. The phase and modulation were determined from a set of 12 phase settings using the manufacturer's software. Resolution of two lifetimes in the frequency domain, pixel by pixel, was performed using the polar plot method (Clayton et al., 2004) again as implemented in the manufacturer's software.

Supplementary Material

Refer to Web version on PubMed Central for supplementary material.

Acknowledgements

This work was supported by grants from the National Health and Medical Research Council of Australia (to RGP and JFH), the Australian Research Council (RGP), and from the US National Institutes of Health. The Institute for Molecular Bioscience is a Special Research Centre of the Australian Research Council. Confocal microscopy was performed at the ACRF/IMB Dynamic Imaging Centre for Cancer Biology, established with the generous support of the Australian Cancer Research Foundation. We are particularly grateful to Professor Ingrid Grummt and Professor Kai Simons for providing constructs. We wish to thank Alun Jones, Adrian Carter and Rachel Hancock for technical assistance. D. A. (PAOOA—111446) and P.W. (PAOOA—109094) are supported by the Swiss National Science Foundation (FNS).

References

- Aboulaich N, Vainonen JP, Stralfors P, Vener AV. Vectorial proteomics reveal targeting, phosphorylation and specific fragmentation of polymerase I and transcript release factor (PTRF) at the surface of caveolae in human adipocytes. *Biochem J* 2004;383:237–248. [PubMed: 15242332]
- Burgener R, Wolf M, Ganz T, Baggiolini M. Purification and characterization of a major phosphatidylserine-binding phosphoprotein from human platelets. *Biochem J* 1990;269:729–734. [PubMed: 2390065]
- Clayton AH, Hanley QS, Verveer PJ. Graphical representation and multicomponent analysis of single-frequency fluorescence lifetime imaging microscopy data. *J Microsc* 2004;213:1–5. [PubMed: 14678506]
- Dawson JC, Legg JA, Machesky LM. Bar domain proteins: a role in tubulation, scission and actin assembly in clathrin-mediated endocytosis. *Trends Cell Biol* 2006;16:493–498. [PubMed: 16949824]
- Drab M, Verkade P, Elger M, Kasper M, Lohn M, Lauterbach B, Menne J, Lindschau C, Mende F, Luft FC, et al. Loss of caveolae, vascular dysfunction, and pulmonary defects in caveolin-1 gene-disrupted mice. *Science* 2001;293:2449–2452. [PubMed: 11498544]
- Fang PK, Solomon KR, Zhuang L, Qi M, McKee M, Freeman MR, Yelick PC. Caveolin-1 alpha and -1 beta perform nonredundant roles in early vertebrate development. *Am J Pathol* 2006;169:2209–2222. [PubMed: 17148682]
- Fra AM, Williamson E, Simons K, Parton RG. De novo formation of caveolae in lymphocytes by expression of VIP21-caveolin. *Proc Natl Acad Sci U S A* 1995;92:8655–8659. [PubMed: 7567992]
- Galbiati F, Engelman JA, Volonte D, Zhang XL, Minetti C, Li M, Hou H Jr. Kneitz B, Edelmann W, Lisanti MP. Caveolin-3 null mice show a loss of caveolae, changes in the microdomain distribution of the dystrophin-glycoprotein complex, and t-tubule abnormalities. *J Biol Chem* 2001;276:21425–21433. [PubMed: 11259414]
- Gustincich S, Vatta P, Goruppi S, Wolf M, Saccone S, Della Valle G, Baggiolini M, Schneider C. The human serum deprivation response gene (SDPR) maps to 2q32-q33 and codes for a phosphatidylserine-binding protein. *Genomics* 1999;57:120–129. [PubMed: 10191091]
- Hagiwara Y, Sasaoka T, Araishi K, Imamura M, Yorifuji H, Nonaka I, Ozawa E, Kikuchi T. Caveolin-3 deficiency causes muscle degeneration in mice. *Hum Mol Genet* 2000;9:3047–3054. [PubMed: 11115849]
- Hailstones D, Sleer LS, Parton RG, Stanley KK. Regulation of caveolin and caveolae by cholesterol in MDCK cells. *J Lipid Res* 1998;39:369–379. [PubMed: 9507997]
- Izumi Y, Hirai S, Tamai Y, Fujise-Matsuoka A, Nishimura Y, Ohno S. A protein kinase C delta-binding protein SRBC whose expression is induced by serum starvation. *J Biol Chem* 1997;272:7381–7389. [PubMed: 9054438]
- Kirkham M, Fujita A, Chadda R, Nixon SJ, Kurzchalia TV, Sharma DK, Pagano RE, Hancock JF, Mayor S, Parton RG. Ultrastructural identification of uncoated caveolin-independent early endocytic vehicles. *J Cell Biol* 2005;168:465–476. [PubMed: 15668297]
- Lichtenberg D, Goni FM, Heerklotz H. Detergent-resistant membranes should not be identified with membrane rafts. *Trends Biochem Sci* 2005;30:430–436. [PubMed: 15996869]
- Monier S, Dietzen DJ, Hastings WR, Lublin DM, Kurzchalia TV. Oligomerization of VIP21-caveolin in vitro is stabilized by long chain fatty acylation or cholesterol. *FEBS Lett* 1996;388:143–149. [PubMed: 8690074]

- Murata M, Peranen J, Schreiner R, Wieland F, Kurzchalia TV, Simons K. VIP21/caveolin is a cholesterol-binding protein. *Proc Natl Acad Sci U S A* 1995;92:10339–10343. [PubMed: 7479780]
- Nichols BJ. A distinct class of endosome mediates clathrin-independent endocytosis to the Golgi complex. *Nat Cell Biol* 2002;4:374–378. [PubMed: 11951093]
- Nixon SJ, Carter A, Wegner J, Ferguson C, Floetenmeyer M, Riches J, Key B, Westerfield M, Parton RG. Caveolin-1 is required for lateral line neuromast and notochord development. *J Cell Sci* 2007;120:2151–2161. [PubMed: 17550965]
- Parolini I, Sargiacomo M, Galbiati F, Rizzo G, Grignani F, Engelman JA, Okamoto T, Ikezu T, Scherer PE, Mora R, et al. Expression of caveolin-1 is required for the transport of caveolin-2 to the plasma membrane. Retention of caveolin-2 at the level of the golgi complex. *J Biol Chem* 1999;274:25718–25725. [PubMed: 10464309]
- Parton RG. Ultrastructural localization of gangliosides; GM1 is concentrated in caveolae. *J Histochem Cytochem* 1994;42:155–166. [PubMed: 8288861]
- Parton RG, Hanzal-Bayer M, Hancock JF. Biogenesis of caveolae: a structural model for caveolin-induced domain formation. *J Cell Sci* 2006;119:787–796. [PubMed: 16495479]
- Parton RG, Molero JC, Floetenmeyer M, Green KM, James DE. Characterization of a distinct plasma membrane macrodomain in differentiated adipocytes. *J Biol Chem* 2002;277:46769–46778. [PubMed: 12356772]
- Pelkmans L, Fava E, Grabner H, Hannus M, Habermann B, Krausz E, Zerial M. Genome-wide analysis of human kinases in clathrin- and caveolae/raft-mediated endocytosis. *Nature* 2005;436:78–86. [PubMed: 15889048]
- Pelkmans L, Puntener D, Helenius A. Local actin polymerization and dynamin recruitment in SV40-induced internalization of caveolae. *Science* 2002;296:535–539. [PubMed: 11964480]
- Pelkmans L, Zerial M. Kinase-regulated quantal assemblies and kiss-and-run recycling of caveolae. *Nature* 2005;436:128–133. [PubMed: 16001074]
- Pol A, Martin S, Fernandez MA, Ingelmo-Torres M, Ferguson C, Enrich C, Parton RG. Cholesterol and fatty acids regulate dynamic caveolin trafficking through the Golgi complex and between the cell surface and lipid bodies. *Mol Biol Cell* 2005;16:2091–2105. [PubMed: 15689493]
- Prior IA, Muncke C, Parton RG, Hancock JF. Direct visualization of Ras proteins in spatially distinct cell surface microdomains. *J Cell Biol* 2003;160:165–170. [PubMed: 12527752]
- Razani B, Wang XB, Engelman JA, Battista M, Lagaud G, Zhang XL, Kneitz B, Hou H Jr, Christ GJ, Edelmann W, Lisanti MP. Caveolin-2-deficient mice show evidence of severe pulmonary dysfunction without disruption of caveolae. *Mol Cell Biol* 2002;22:2329–2344. [PubMed: 11884617]
- Tagawa A, Mezzacasa A, Hayer A, Longatti A, Pelkmans L, Helenius A. Assembly and trafficking of caveolar domains in the cell: caveolae as stable, cargo-triggered, vesicular transporters. *J Cell Biol* 2005;170:769–779. [PubMed: 16129785]
- Thomsen P, Roepstorff K, Stahlhut M, van Deurs B. Caveolae are highly immobile plasma membrane microdomains, which are not involved in constitutive endocytic trafficking. *Mol Biol Cell* 2002;13:238–250. [PubMed: 11809836]
- Vinten J, Johnsen AH, Roepstorff P, Harpoth J, Tranum-Jensen J. Identification of a major protein on the cytosolic face of caveolae. *Biochim Biophys Acta* 2005;1717:34–40. [PubMed: 16236245]
- Vinten J, Voldstedlund M, Clausen H, Christiansen K, Carlsen J, Tranum-Jensen J. A 60-kDa protein abundant in adipocyte caveolae. *Cell Tissue Res* 2001;305:99–106. [PubMed: 11512676]
- Voldstedlund M, Thuneberg L, Tranum-Jensen J, Vinten J, Christensen EI. Caveolae, caveolin and cav-p60 in smooth muscle and renin-producing cells in the rat kidney. *Acta Physiol Scand* 2003;179:179–188. [PubMed: 14510782]
- Voldstedlund M, Vinten J, Tranum-Jensen J. cav-p60 expression in rat muscle tissues. Distribution of caveolar proteins. *Cell Tissue Res* 2001;306:265–276. [PubMed: 11702238]
- Wanaski SP, Ng BK, Glaser M. Caveolin scaffolding region and the membrane binding region of SRC form lateral membrane domains. *Biochemistry* 2003;42:42–56. [PubMed: 12515538]
- Way M, Parton RG. M-caveolin, a muscle-specific caveolin-related protein. *FEBS Lett* 1995;376:108–112. [PubMed: 8521953]
- Williams TM, Lisanti MP. Caveolin-1 in oncogenic transformation, cancer, and metastasis. *Am J Physiol Cell Physiol* 2005;288:C494–506. [PubMed: 15692148]

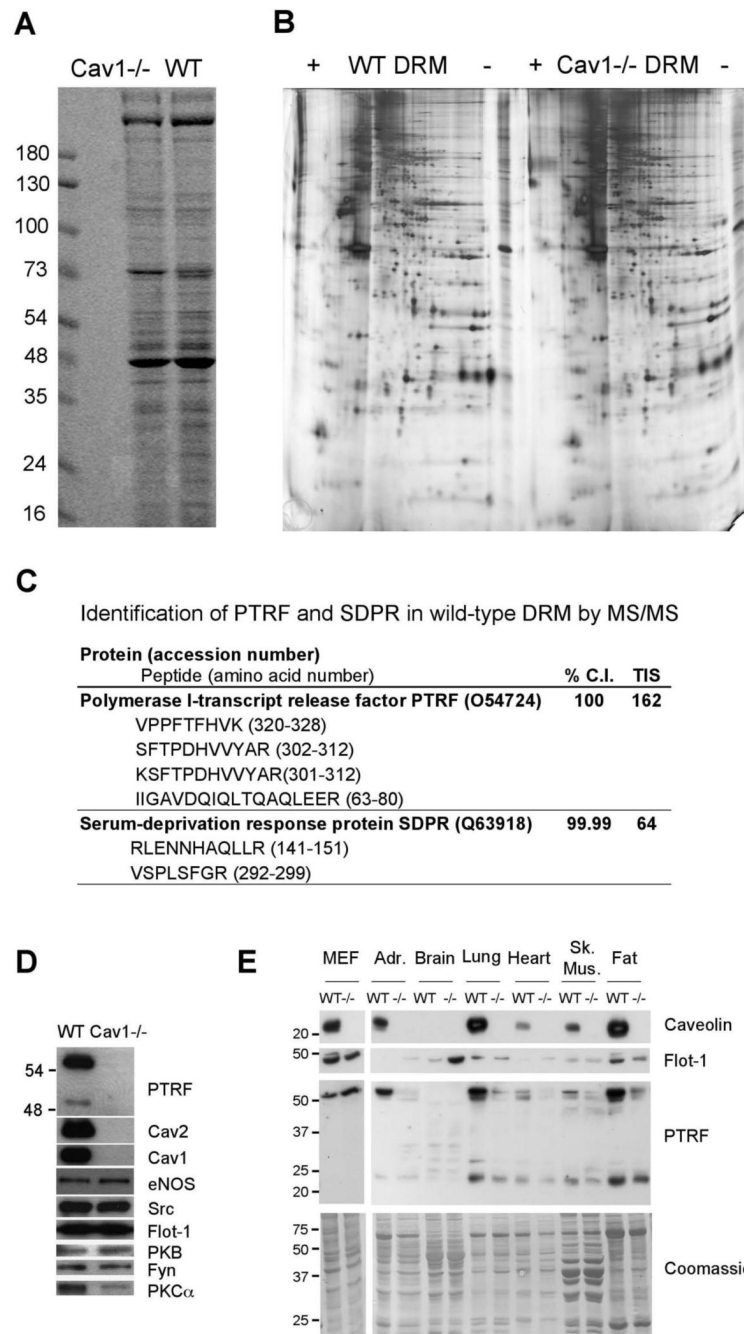


Figure 1. Identification of PTRF as a protein enriched in Cav1-containing DRM.

DRM prepared from WT and Cav1^{-/-} MEF were analysed by (A) SDS-PAGE (5-15%) and colloidal Coomassie staining or (B) 2D gel electrophoresis (pH3-10, 12%) and silver staining. (C) Slices from a 12% colloidal Coomassie-stained SDS-PAGE gel were digested with trypsin and analysed by mass spectrometry. PTRF and SDPR were identified in WT but not Cav1^{-/-} DRM. %C.I (% Confidence Interval) and TIS (Total Ion Score) from Mascot searches are shown.

(D) The enrichment of PTRF in WT DRM was confirmed by western blotting and compared with selected signaling proteins.

(E) Expression of PTRF, caveolin and flotillin-1 was examined by western blotting in MEF and adult tissue lysates prepared from WT and Cav1^{-/-} mice. Twenty μ g of each lysate was loaded and the membrane was Coomassie stained to confirm protein loading. The blots are representative of two independent tissue lysates. SDS-PAGE molecular weight markers are shown in kDa. Adr, adrenal gland; Sk. Mus, skeletal muscle.

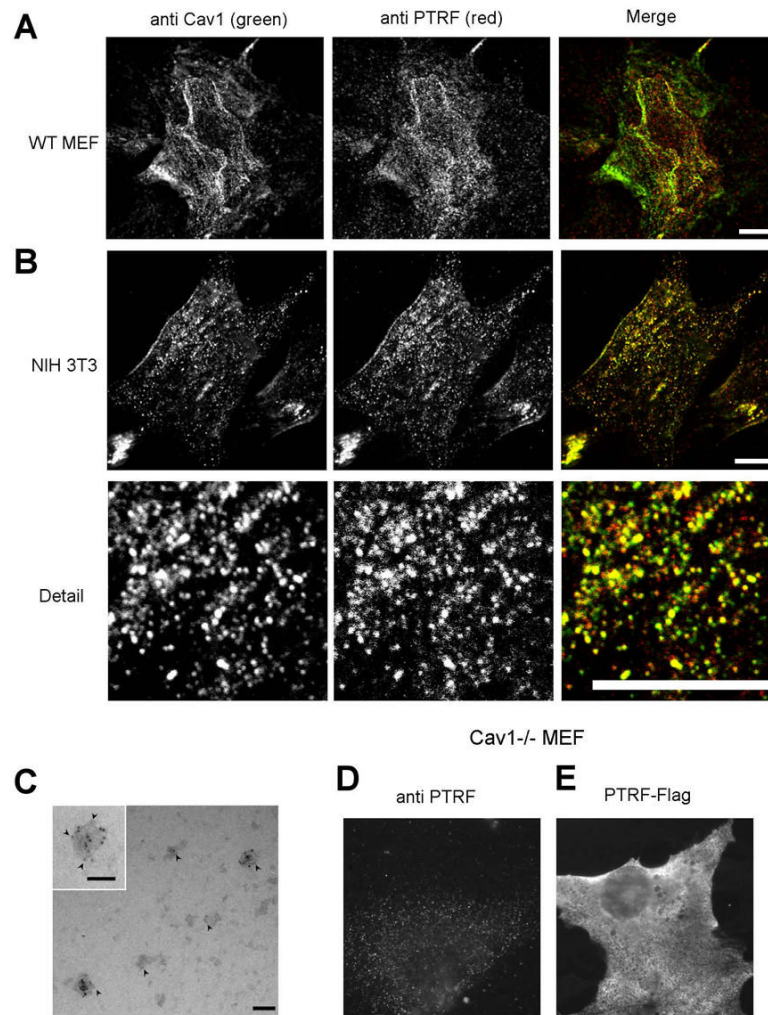


Figure 2. PTRF associates with caveolae

(A) WT MEF and (B) NIH 3T3 fibroblasts grown on coverslips were labelled for endogenous Cav1 and PTRF, then examined by confocal microscopy. In both cell types Cav1 and PTRF show extensive colocalization in cell surface puncta. Bars, 10 μ m.

(C) Immuno-EM of plasma membrane sheet shows co-labelling of Cav1-GFP (5 nm gold) with PTRF-RFP (2 nm gold; arrowheads) in co-transfected BHK cells. Bar, 100 nm.

(D) Cav1^{-/-} MEF labelled for endogenous PTRF, or (E) transfected with PTRF-Flag and labelled for the Flag tag show diffuse labeling of PTRF. Bars, 10 μ m.

Live cell images of GFP-PTRF in unfixed WT and KO MEF are available in Figure. S1.

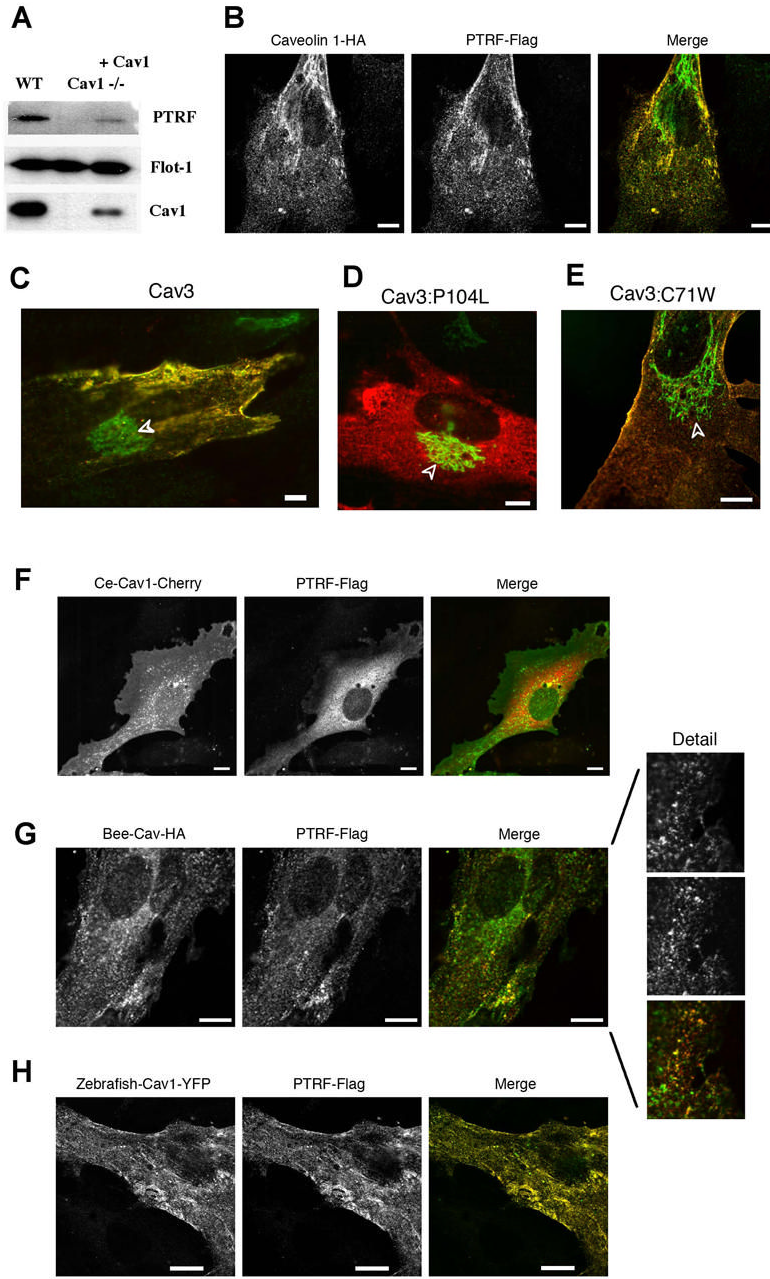


Figure 3. Cav1 expression is sufficient to recruit PTRF to DRM; PTRF is recruited to the cell surface by caveolae-generating forms of Cav1 and Cav3 but is not recruited to caveolin at the Golgi complex

(A)DRMs prepared from WT MEF, Cav1^{-/-} MEF, and Cav1^{-/-} MEF in which Cav1 was re-expressed by infection with adenovirus-Cav1, was analyzed by western blotting for PTRF, Flotillin-1 and Cav1.

(B-H) Cav1^{-/-} MEF co-transfected with PTRF-Flag and Cav1-HA (B), Cav3-HA (C), Cav3 P104L-HA (D), Cav3 C71W-HA (E), *C. elegans* caveolin (Ce-Cav1-Cherry, panel F), *Apis mellifera* caveolin (Bee-Cav-HA; panel G) or zebrafish-Cav1-YFP (panel H) were fixed, labelled with anti-Flag antibody and anti-HA antibody where required. The localization of expressed PTRF and caveolin was examined by confocal microscopy. Note that *C. elegans*

Cav1 (Ce-Cav1-Cherry) associates with the cell surface but does not generate caveolae (unpublished results) and does not recruit PTRF to the plasma membrane. Bars, 10 μ m.

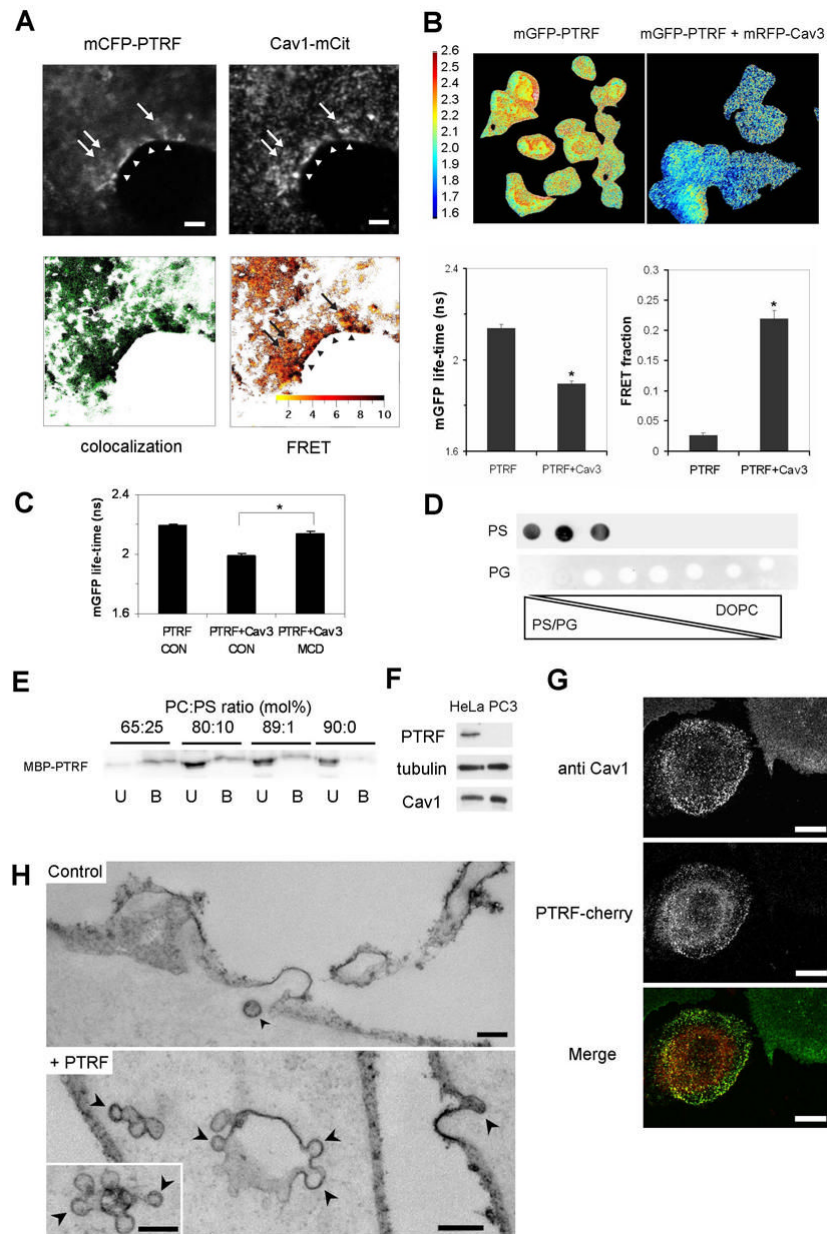


Figure 4. PTRF and caveolin interact in a cholesterol-dependent manner. PTRF is required for caveolae formation in PC3 cells

(A) BHK cells were transiently transfected with mCFP-PTRF and mCit-Cav1. The distribution of mCFP-PTRF is observed in the donor channel and mCit-Cav1 in the acceptor channel image. FRET was observed in vesicular structures along the plasma membrane (arrowheads) and at the cell periphery (arrows). FRET was calculated per pixel as a sensitized acceptor emission index FR, ranging from 1 (no FRET) to 10. Overlay of a binary colocalization image (green pixels) and a binary FRET image showing all pixels with FR>2 in black, revealed that all structures where mCFP-PTRF and mCit-caveolin-1 colocalized also exhibited FRET. Bars, 2 μ m.

(B) BHK cells transiently expressing mGFP-PTRF with, or without mRFP-Cav3 were imaged in a wide-field FLIM microscope. Representative FLIM images are shown and the fluorescence lifetime (ns) of mGFP displayed as a heat map. In the presence of the acceptor mRFP the

lifetime of the donor mGFP is significantly decreased; this was quantified by calculating the mean lifetime of mGFP on a cell by cell basis (mean \pm SEM, $n \geq 50$ cells from three independent experiments). The reduced mGFP lifetime reflects FRET between mGFP and mRFP as a result of the molecular proximity of PTRF and Cav3. The fraction of donor fluorophores undergoing FRET was extracted from the FLIM data (see Experimental Procedures). * $p < 0.0001$.

(C) FLIM experiment was performed as described for (B), except that cells were treated with 1% Methyl- β -cyclodextrin for 20 min (MCD) or left untreated (CON). * $p < 0.001$.

(D) PTRF binding to phosphatidylserine (PS) in a solid-phase assay. Each spot contained 2 μ g of phospholipid with gradual decrease of the anionic phospholipid content as indicated. Binding of PTRF was detected by immunoblotting. PG, phosphatidylglycerol, DOPC, dioleoylphosphatidylcholine.

(E) PTRF binding to acidic phospholipids was assayed by co-sedimentation with liposomes containing decreasing amounts of phosphatidylserine (PS, mass balanced by phosphatidylcholine, PC). U, unbound fraction, B, bound fraction. Binding of PTRF is essentially absent in liposomes lacking PS.

(F) The protein levels of PTRF and Cav1 was examined by immunoblotting in 10 μ g of total cell lysates from HeLa and PC3 cells. Tubulin was used as a loading control.

(G) PC3 cells grown on glass coverslips were transfected with PTRF-cherry, and labelled for endogenous Cav1. The example image shows one transfected cell (left) and one untransfected cell (right) in the same field.

(H) Control or PTRF-transfected PC3 cells were fixed in the presence of ruthenium red to label the cell surface, and examined by electron microscopy. Control cells show few uncoated invaginations with the morphology of caveolae; note the 120nm coated vesicle (arrowhead). In transfected cells, numerous uncoated pits (arrowheads) with the typical morphology of single caveolae and caveolae rosettes are evident. Caveolae density increased from 0.26 ± 0.13 caveolae per field in control cells to 1.70 ± 0.94 in PTRF transfected cells. Transfection efficiency was approximately 50%. Bars, 200nm.

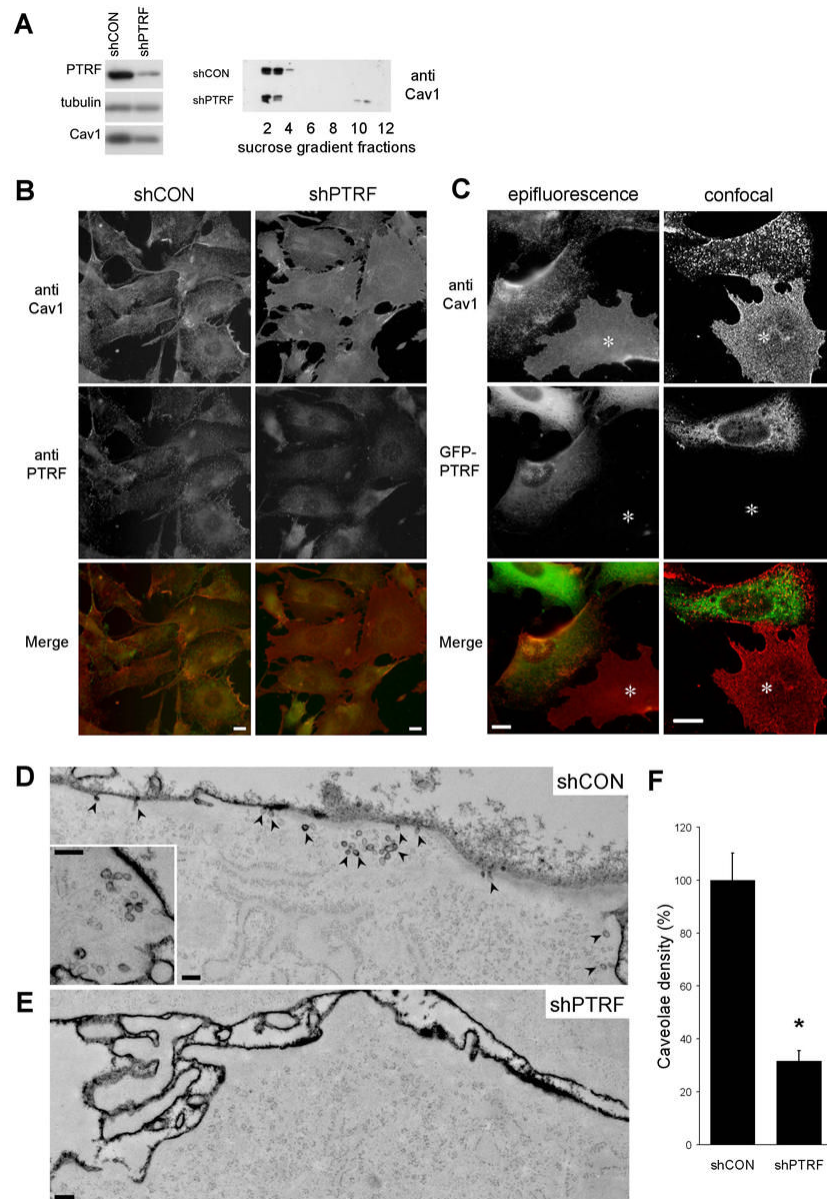


Figure 5. PTRF knockdown reduces caveolae density in NIH 3T3 cells

NIH 3T3 fibroblasts were transfected with shRNA to PTRF (shPTRF) or control shRNA (shCON). Stable cell lines were generated by selection in G418.

(A) shPTRF cells show reduction of PTRF expression without affecting Cav1 association with DRMs on sucrose gradient.

(B) Immunofluorescence labeling of methanol-fixed shCON and shPTRF cells shows punctuate Cav1 labeling in shCON cells and diffuse labeling in shPTRF cells. Note that PTRF antibody labeling is weak under these conditions which were optimized to show the differential Cav1 labeling in the two cell types. Bars, 1 μ m.

(C) shPTRF NIH 3T3 fibroblasts were transfected with PTRF-GFP and then labelled for Cav1. In transfected cells Cav1 shows the characteristic punctate staining seen in WT MEF, NIH 3T3 and shCON cells, whereas untransfected cells (asterisks) show diffuse labeling for Cav1. Bars, 1 μ m.

(D-F) To quantitate surface caveolae, shCON cells (D) or shPTRF cells (E) were surface-labeled by fixation in the presence of ruthenium red. Abundant caveolae, surface pits of approximately 65nm diameter, are evident close to the surface of shCON cells (arrowheads) but rarely in shPTRF cells. Caveolae density was quantitated (F) from three independent experiments as described in Experimental Procedures.* $p < 0.005$ Bars, 200 nm.

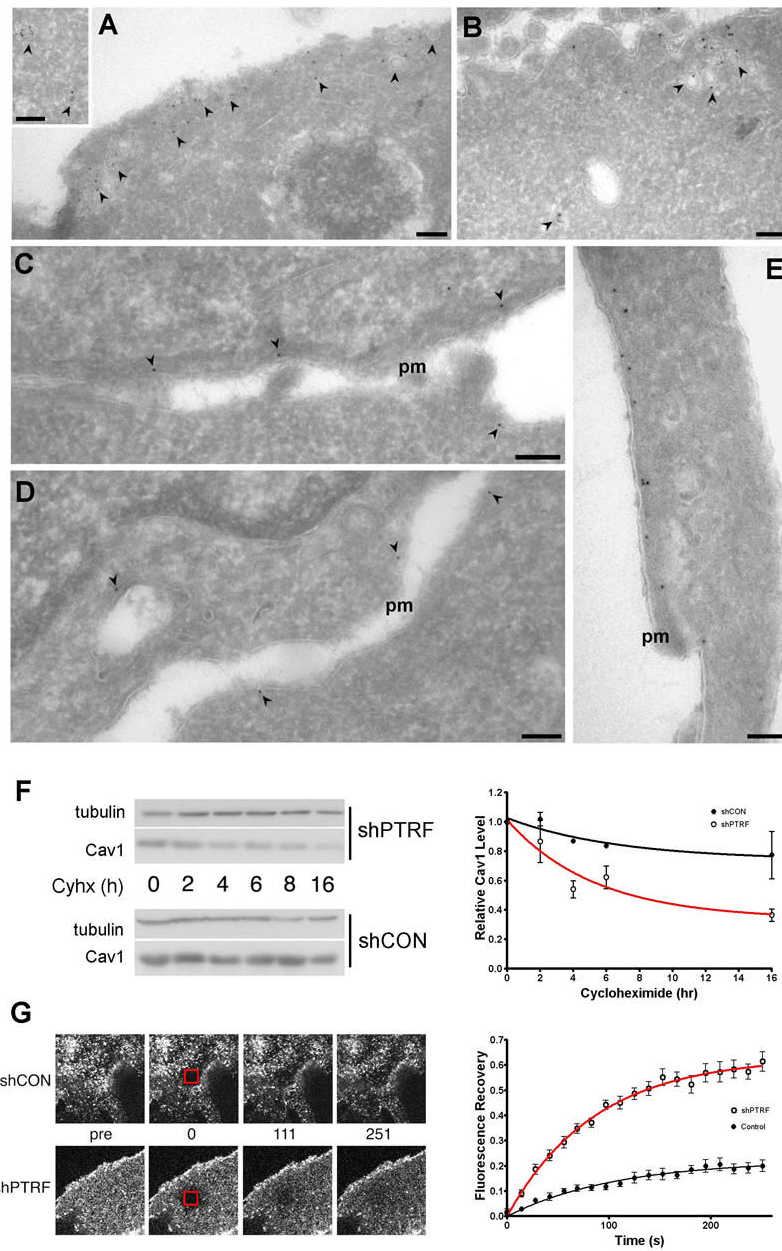


Figure 6. PTRF knockdown causes redistribution of Cav1 to non-caveolar membrane, increases the Cav1 degradation and lateral mobility at the plasma membrane

Localization of Cav1 was examined in shCON (A-B) and shPTRF (C-E) cells by quantitative immunoelectron microscopy on frozen sections. In control cells, $81.7 \pm 4.6\%$ of surface caveolin was associated with 65nm vesicles close to, or clearly connected to the plasma membrane (arrowheads A,B). In contrast, $79.1 \pm 5.3\%$ of surface caveolin labelling was associated with non-caveolar membrane in shPTRF cells. Bars, 200nm. pm, plasma membrane.

(F) PTRF knockdown accelerates the degradation of Cav1. shPTRF and shCON cells were treated with 10 μ M cycloheximide for the indicated times, and the level of Cav1 protein assessed by immunoblotting whole cell lysates. Tubulin was used as a loading control. Graph represents data from two independent experiments.

(G) PTRF knockdown results in a highly significant increase ($p < 0.001$) in the mobile fraction of Cav1. Control and shPTRF fibroblasts were transiently transfected with YFP-Cav1. A $36 \mu\text{m}^2$ area of the cell (boxed in the second image) was bleached to background levels and images were then captured at 14 second intervals. The mean of normalised data from 10 independent FRAP experiments per cell type are plotted and the τ_d and R_f derived from a one-phase exponential association fit to the data. The half life (τ_d) for shCON was not significantly different from shPTRF (74 sec and 60 sec, respectively).

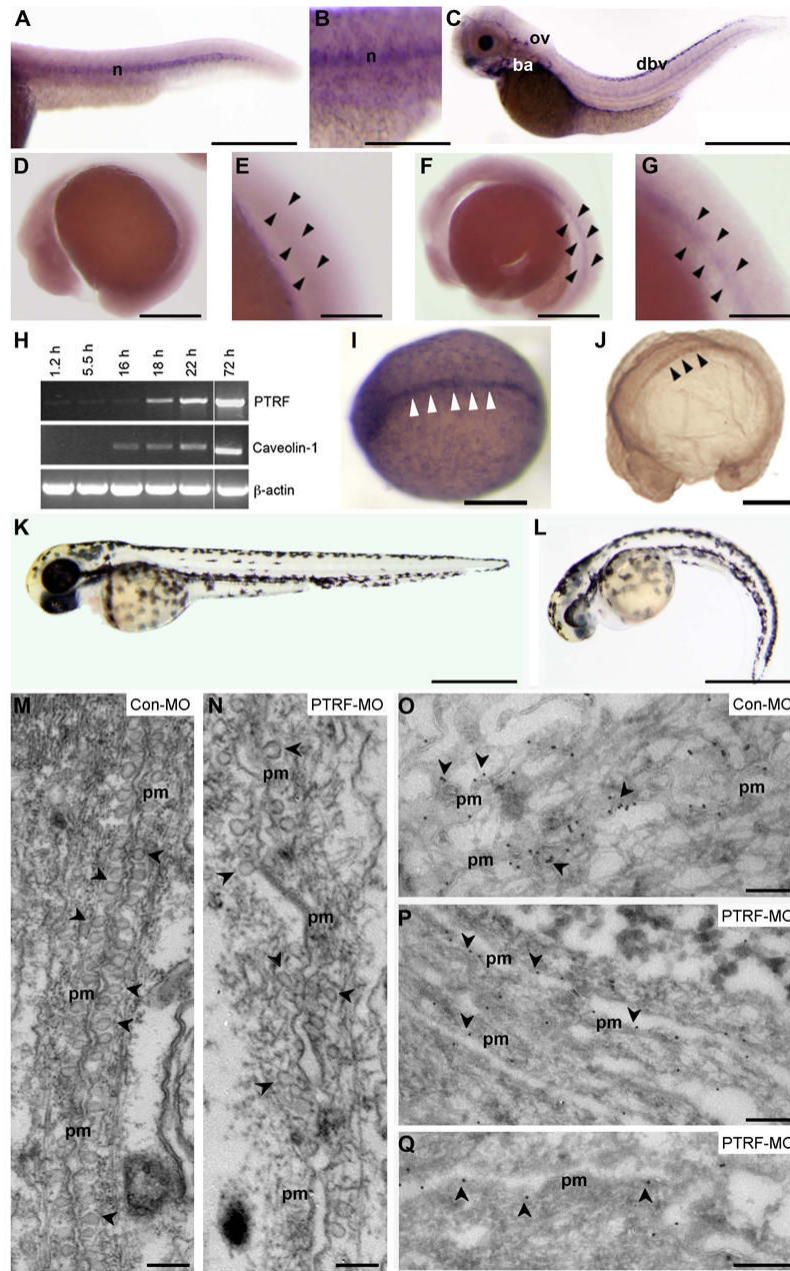


Figure 7. PTRF is required for caveolae formation in zebrafish notochord cells

(A-G) Expression pattern of PTRF during zebrafish development was analysed by wholemount mRNA *in situ* hybridisation. Anterior is to the left and dorsal to the top. PTRF expression was detected in the notochord (n) in 24h embryos (A) and 31h embryos (B). In 72h embryos (C), expression was detected in dorsal blood vessels (dbv), in the otic vesicle (ov) and in the branchial arches (ba). PTRF mRNA expression was first detected in 18h embryos (F, G) and it was not detected in 16h embryos (D, E).

(H) RT-PCR comparing the temporal mRNA expression pattern of PTRF and Cav1 during early embryo development. PTRF mRNA expression arose at 18h and was maintained throughout the development until 72h. Cav1 mRNA expression was detected earlier than PTRF, and was detected in the notochord as early as 12h by *in situ* hybridisation (I). Expression

of Cav1 protein was observed in the notochord by immunohistochemistry of 16h embryos (J). Arrowheads in A-J indicate the notochord. (K, L) PTRF knockdown embryos were generated by morpholino (MO) injection (6 ng/embryo). At 48h, 79% of control MO injected embryos appeared normal (K), whereas 44% of embryos injected with PTRF MO were curved under and/or presented heart edema (L).

(M-Q) Ultrastructural analysis and immunogold labeling of the notochord of 48h embryos injected with control MO (M, O) or PTRF MO (N,P,Q). In the regions of cell-cell contact, the plasma membranes (PM) of neighbouring cells are closely apposed. The plasma membrane in these regions is covered in caveolae (some of which are indicated by arrowheads) in the control MO-injected embryos (M). Caveolin immunogold labeling (arrowheads) is associated with the invaginated caveolae as seen in frozen sections labeled in parallel (O). The density of caveolae is greatly reduced in PTRF MO-injected embryos (N) and the plasma membranes of neighbouring cells are less closely apposed. Caveolin labeling is associated predominantly with flat plasma membrane rather than invaginated caveolae in the PTRF MO-injected embryos (P,Q). pm, plasma membrane. Scale bars (A, B, C, D, F, I, J, K, L) 250 μ m, (E, G) 80 μ m and (M-Q) 200 nm.